Published in final edited form as:
Proteins. 2009 May 1; 75(2): 499–508. doi:10.1002/prot.22265.

PIK3CA somatic mutations in breast cancer: Mechanistic insights from Langevin dynamics simulations

Parminder K. Mankoo[1], **Saraswati Sukumar**[2], and **Rachel Karchin**[1,*]

[1] Department of Biomedical Engineering and Institute for Computational Medicine, Johns Hopkins University, Baltimore, Maryland 21218

[2] Department of Oncology, Johns Hopkins University School of Medicine, Baltimore, Maryland 21231

Abstract

Somatic mutations in PIK3CA (phosphati-dylinositol-3 kinase, catalytic subunit, alpha isoform) are reported in breast and other human cancers to concentrate at hotspots within its kinase and helical domains. Most of these mutations cause kinase gain of function *in vitro* and are associated with oncogenicity *in vivo*. However, little is known about the mechanisms driving tumor development. We have performed computational structural studies on a homology model of wildtype PIK3CA plus recurrent H1047R, H1047L, and P539R mutations, located in the kinase and helical domains, respectively. The time evolution of the structures show that H1047R/L mutants exhibit a larger area of the catalytic cleft between the kinase N- and C-lobes compared with the wildtype that could facilitate the entrance of substrates. This larger area might yield enhanced substrate-to-product turnover associated with oncogenicity. In addition, the H1047R/L mutants display increased kinase activation loop mobility, compared with the wildtype. The P539R mutant forms more hydrogen bonds and salt-bridge interactions than the wildtype, properties that are associated with enhanced thermostability. Mutant-specific differences in the catalytic cleft and activation loop behavior suggest that structure-based mutant-specific inhibitors can be designed for PIK3CA-positive breast cancers.

Keywords

kinase inhibitors; gain of function; oncogenicity; hot spot; molecular modeling; missense mutations

INTRODUCTION

A recent development in breast cancer research has been the discovery that the catalytic subunit of the gene phosphatidylinositol-3 kinase (PI3K) called PIK3CA or p110α is frequently mutated in breast cancer.[1–3] Among 210,000 breast cancers diagnosed each year in the United States alone, about 70,000 cases (30%) are estimated to carry somatic mutations in PIK3CA.[4] Experimental studies have shown that the most frequently observed "hot spot" PIK3CA mutations in human cancers are associated with increased kinase activity in the PI3K pathway and growth in soft agar *in vitro*.[5,6] Studies in chicken embryo membranes and nude mice have shown that these PIK3CA mutations are oncogenic *in vivo*,

*Correspondence to: Rachel Karchin, Department of Biomedical Engineering and Institute for Computational Medicine, Johns Hopkins University, 217A CSEB Building, 3400 North Charles Street, Baltimore, MD 21218. karchin@jhu.edu.

driving tumor development by constitutive activation of the PI3K pathway.[4,5] This discovery poses a number of clinically and structurally relevant questions. How do particular PIK3CA mutations hyperactivate the PI3K pathway? What are the structurally important conformational changes that could guide mutant-specific development of inhibitors? Here, we describe a computational structural investigation that begins to address these questions.

There are three main classes (Class I–III) of PI3Ks, grouped according to substrate specificity and homology. The Class IA PI3Ks (PIK3CA, PIK3CB, PIK3CD) are heterodimeric lipid kinases composed of a p110 catalytic and a p85 regulatory subunit.[7] The catalytic subunit of PIK3CA is composed of several modular domains: kinase domain, helical domain, C2 domain, Ras-binding domain, and the N-terminal domain (P85-binding domain), which interacts with the p85α regulatory subunit. The kinase domain has two lobes: an N-terminal lobe, consisting of a five-stranded beta sheet flanked by three alpha helices, and a primarily helical C-terminal lobe. The reaction catalyzed by PIK3CA consists of transfer of the γ-phosphate of adenosine-5′-triphosphate (ATP) to the 3′ hydroxyl group of the inositol ring of phosphatidylinositol-4,5-bisphosphate (PIP_2), converting it into phosphatidylinositol-3,4,5-triphosphate (PIP_3).4,7,8 An ATP cofactor binds between the kinase lobes in a manner similar to protein kinases, with many of the enzyme/ATP contacts involving amino acid residues in a loop that links the two lobes.[7,9] In the PI3K signaling pathway (Fig. 1A), PIK3CA phosphorylation of PIP_2 is balanced by the phosphatase and tensin homolog (PTEN), which converts PIP_3 back into PIP_2. Hyperactive PIK3CA and underactive PTEN both result in elevated levels of PIP_3, which functions as a second messenger, activating the tyrosine kinase AKT (v-akt murine thymona viral oncogene) and consequently multiple downstream signaling pathways that regulate cellular growth, transformation, adhesion, apoptosis, survival, and motility.[4,6] Although PI3K pathways were known to be hyperactivated in human tumors, until recently the PI3Ks were thought to play a passive role, as targets of increased receptor tyrosine kinase signaling.[4,6,11]

The PIK3CA somatic mutations found in tumor sequencing studies[1,12] do not map randomly over the extent of the gene, but are concentrated at distinct hot spots (Fig. 1B). This fact suggests that they may drive tumor progression[2,13,14] by conferring a gain of function to PIK3CA. Studies in MCF10A immortalized breast epithelial cell lines show that the most frequently observed PIK3CA mutations in human breast cancers (E545K in exon 9 and H1047R in exon 20)[2,14] are associated with increased kinase activity in the PI3K pathway. Chorioallantoic membrane assays in chicken embryos confirm that these mutations (including H1047L and P539R) are oncogenic *in vivo*.[11,15]

In general, protein and lipid kinases have “closed” and “open” states characterized by conformational differences @in the activation loop and relative positioning of the N- and C-lobes.[16] The activation loop of PI3Ks is considered to be a topological counterpart of the activation loop of the protein kinases.[17] It is connected to a highly conserved kinase domain sequence motif (DFG). Pirola *et al*.[17] suggested that PI3K activation loops tend to be disordered, assuming well-defined structure only upon PIP_2 binding, thus yielding a “closed” state that reduces the solvent accessibility of the catalytic pocket.

X-ray crystallography and molecular dynamics studies have previously been used to explore the role of activation loops in protein and lipid kinases,[18–20] but not in members of the PI3K family. However, a recent *in vitro* study in HEK293T (hamster embryonic kidney) cells found elevated lipid kinase activity in several PIK3CA mutants that lie near the activation loop and speculated that the increase was related to changes in its conformation.[21] Several biochemical studies of PIK3CA have used homology models based on the X-ray crystal structure of porcine PIK3CG (a Class 1B PI3K).[4,9,17]

Homology models have been criticized for inaccuracy due to bias towards the structure used as a template, lack of water molecules, and insufficient resolution to correctly position sidechains (reviewed in Refs. 22, 23). However, despite these inherent drawbacks, homology modeling has become a standard tool in structural biology. The combined use of homology models and molecular dynamics has been previously used successfully to study complex biological processes such as potassium ion channels and has yielded experimentally verifiable results.[24–26] Implicit solvent models have also successfully approximated explicit solvent behavior in complex phenomena such as conformational changes and ligand-protein binding.[27–29] In this study, we explore a large protein (~1000 amino acid residues) with Langevin dynamics (LD) in implicit solvent, using a homology model as the initial structure.

METHODS AND MATERIALS

Homology modeling

For our structural analysis, we built a homology model of wildtype PIK3CA using MODELLER 9.1 and the MODPIPE 2.0 protocol.[30–32] We used MODELLER's BUILDPROFILE and PROFILE-PROFILE-SCAN modules to: (1) build a sequence profile based on the PIK3CA human sequence (UniProt P42336); (2) select the best available template by scanning a sequence profile library of proteins in protein data bank (PDB) (filtered to remove sequences with >95% sequence identity); and (3) align the profiles of PIK3CA and the selected template sequence. The selected template was porcine PIK3CG (PDB: 1E7U)[9] (2.0 Å resolution, Rfree 0.298). This template has 37% sequence identity with human PIK3CA (alignment shown in Fig. 2). We used MODELLER to construct an ensemble of 100 models and selected the one with the best objective function. The kinase domain activation loop, which contains disordered regions in the 1E7U structure, was modeled with MODELLER's standard loop building routines.[34,35] We assessed model quality using atomic nonlocal environment assessment (ANOLEA)[36] and protein structural analysis (ProSA)-web.[37] CHARMM software (c32b1 with CHARMM22 force field)[38] was used to build atomic coordinates of the mutants R1047, L1047, and R539. Homology modeling was done on a Dell Precision 690 PC running Fedora Core 5 Linux. CHARMM was run on an IBM p690 using the AIX operating system.

LD simulations

To explore conformational changes differing among wildtype and mutant PIK3CAs, we ran 5 ns LD simulations (with friction coefficient of 10 ps^{-1}) using CHARMM (c32b1) with CHARMM22 force field and the generalized born molecular volume (GBMV) implicit solvent model.[39,40] LD is a type of molecular dynamics that is well suited to large biomolecules, because it is based on a simplified, stochastic model of the collisions of protein atoms with solvent molecules and frictional forces (reviewed in Ref. 41). These simplifications reduce the computational time required, when compared with expensive explicit solvent dynamics simulations. LD has been used to examine both equilibrated thermodynamic properties and kinetic properties in a wide range of systems and has been shown to effectively replicate behavior seen in explicit solvent simulations.[41–43] It also provides an effective thermostat with a temperature that is controlled through the magnitude of the random forces. In these simulations, a modified equation of motion is applied for a single particle *i*:

$$m_i a_i = F_i(\vec{r}) - g_i m_i v_i F_{\mathrm{RANDOM}}(t) \quad (1)$$

where *m*, *a*, *v*, and *F* are the mass, acceleration, velocity, and the force due to the interactions with the rest of the system, *g* is the friction coefficient, and F_{RANDOM} is a stochastic force modeling random collisions with the solvent atoms. Simulations were performed with a 2 fs time step at a constant temperature of 300 K, using the SHAKE algorithm[44] applied to all hydrogen bond lengths. Before dynamics, we minimized the structures in vacuum with a harmonic constraint of 5 kcal/mol/Å^2 on the backbone atoms. Side-chains were allowed to move without restraints. The system was minimized with 200 steps of Steepest Descent algorithm, followed by Adopted Basis Newton Raphson as implemented in CHARMM[45] until tolerance applied to the average gradient in energy was $\leq 10^{-4}$ and further minimized in GBMV implicit solvent by gradually relaxing the backbone harmonic constraint from 5 to 0.1 kcal/mol/Å^2. The resulting ensemble was then equilibrated for 1 ps with a backbone harmonic constraint of 0.1 kcal/mol/Å^2, followed by unrestrained equilibration for 1 ps. The production runs were performed with the list of nonbonded interactions truncated at 18 Å and nonbonded van der Waals interaction switched off at 11–14 Å. Coordinates were saved every 4 ps. All simulations were run on an IBM p690 using the AIX operating system.

PIK3CA holo model with ATP bound

To explore how ATP interacts with the N- and C-lobes of the kinase domain, we constructed an initial structure by mimicking its location in the PIK3CG X-ray crystal structure (PDB: 1E8X).[9] Simulation protocols were the same as described above except that harmonic constraints were also applied to ATP during minimization and equilibration. The production run was performed for 2.0 ns.

RESULTS

We selected the cancer-related PIK3CA missense mutations H1047R, H1047L, and P539R for LD simulations. Two of these mutants are near the activation loop and one is in the helical domain. The structure of human PIK3CA was unknown when our study began, and we built a homology model (Fig. 1C) to use as the initial structure for our LD simulations of wildtype and three mutants: H1047R, H1047L, and P539R (without ATP) and holo mutant H1047R (with ATP).

Homology model validation

Initial model assessment suggested that our homology model was of good quality. The model's ProSA Z-score[37] was −8.86, indicating that the number of errors in the model was in a similar range to that of experimentally determined structures of a similar size (961 residues) found in the PDB. Position-specific assessment with ANOLEA[36] showed that areas in the C2 domain and the loops connecting C2 and helical domains were poor, however, these regions were not the focus of our analysis. Towards the end of our study, the first X-ray crystal structure of PIK3CA (PDB: 2RD0) with resolution of 3.05 Å was released.[46] We did a structural alignment of this structure and our homology model (Cα atoms only in regions of regular secondary structure), yielding 701 equivalent positions (of 986 residues in the homology model) and 2.02 Å root-mean-squared deviation (RMSD), further supporting the utility of our homology model. The RMSD calculation was done with the align3d and superpose routines in MODELLER 9.1, using default parameters and an in-house PYTHON script. Generally, the distribution of per-residue RMSD is lower in the range from amino acid residue positions 500–1061, which correspond to the helical and kinase domains that are the subject of our study. Importantly, in a low resolution X-ray structure (>2.5 Å), the subjective interpretation of the crystallographer plays a large role in translating the electron density map into atomic coordinates. In a typical structure with

resolution >3.0 Å, the uncertainty of individual atom positions can be 0.5 Å or more.[47] The 2RD0 structure does not contain bound ATP or the activation loop.

Two distinct gain-of-function mechanisms

Our simulations support the possibility that H1047R/L and P539R, which occur in the kinase and helical domains of PIK3CA, respectively, could induce enzymatic gain-of-function by different mechanisms. We observe that (1) the H1047R/L mutations cause a substantial increase in activation loop fluctuations when compared with P539R and wildtype; (2) the H1047R/L mutations induce an increase in solvent accessible surface area of the active site cleft, whereas P539R induces a slight decrease in solvent accessible surface area, and wildtype has no impact on it; (3) the P539R mutant might increase thermostability, compared with wildtype, as measured by number of hydrogen bonds and salt-bridge interactions over the time course of our simulations.

Fluctuations in activation loop

The activation loop amino acid residues fluctuate between 3 and 4 Å RMSD, with respect to initial structures at 0 ps, for the entire 5 ns of the production run for wildtype and P539R. In contrast, these residues undergo large fluctuations in the H1047R and H1047L mutants (Fig. 3A).

Conformational changes in kinase domain N- and C-lobes

To compare kinase domain N- and C-lobe movements among wildtype and mutants, we measured changes in solvent accessible surface area for the region between the two lobes over the course of each simulation (Fig. 3B). For wildtype, the solvent accessible surface area remains constant, at approximately 105 nm^2. In H1047R and H1047L mutants, solvent accessible surface area increases substantially to 116 and 120 nm^2, respectively. The P539R mutant shows a decrease in solvent accessible surface area over the course of the simulation from 110 to 107 nm^2.

Thermostability of mutants compared with wildtype

To estimate possible changes in thermostability of PIK3CA upon mutation, we measured the number of hydrogen bonds and salt bridges of the wildtype and mutants during the simulations. On average, H1047R/L has 227 hydrogen bonds and P539R has 230, compared with 223 for the wildtype. The P539R mutation also induces a salt-bridge triad between E600, R539, and D603, which forms at the beginning of the production run (Fig. 4A). At 5 ns, the P539R mutant has 88 salt bridges (wildtype has 80).

P539R mutation induces long-range conformational changes

At 0 ns, E453 (C2-domain) interacts with F1016 (kinase domain) at the tri-domain interface (C2, kinase, and helical) (Fig. 4B). An electrostatic attraction between R539 and E453 develops over the course of the dynamics simulation and F1016 moves away from the interface, whereas H450 (C2 domain) moves towards D1018. The overall effect of these conformational changes apparently pulls the C2 domain closer to the helical domain. The C2 domain is believed to play a role in membrane binding and substrate targeting.[9,48] However, probing how the P539R mutant will affect the membrane binding of PIK3CA will require further molecular modeling studies that include the membrane environment.

H1047R mutant induces a phenylalanine flip

In the wildtype, F934 sits in a pocket closely interacting with amino acid residues forming the catalytic loop, pointing away from the catalytic cleft. The conformational change in R1047 perturbs the hinge region of the activation loop and subsequently reorganizes the

network of interactions between activation loop and catalytic loop (see Fig. 5). At 0 ns, R916 in the catalytic loop forms a hydrogen bond with D933 of the DFG-motif. In the time course of the simulation, this hydrogen bond is broken, resulting in a ~90° rotation of D933. As a result, F934, which originally pointed towards the interior of the protein, flips and becomes more exposed.

ATP binding

The binding mode of ATP in PIK3CA is not yet known. Although an X-ray crystal structure of PIK3CG with ATP bound is available in PDB, the recently published structure of PIK3CA[46] is missing ATP (PDB: 2RD0). We explored possible ATP binding interactions with our homology model (Methods). Although we made no *a priori* assumptions about hydrogen bonding, during the time course of our simulations, the ATP formed hydrogen bonds with several residues [ATP(N1)-V851(HN), ATP(O2B)-S774(HG1)] (see Fig. 6). ATP (O2A, O2B) also formed hydrogen bonds with the K802 (HZ1) residue, which is involved in a salt bridge with D933 (of the DFG-motif). These hydrogen bonds are generally conserved in the kinase superfamily.[49] Intermittently, the ATP (N6) amino group also hydrogen bonded with the carbonyl backbone of E849. The structure of the H1047R mutant with bound ATP was stable for the entire length of the simulation.

Assessment of LD simulations

The time profiles of main chain heavy atoms' RMSD, relative to the initial structure, plateau in all simulations at approximately 3.25 ns (Fig. 3C). The converged total energies of all the mutants and the wildtype are shown over the last 1 ns of the simulations (Fig. 3D). Average energy contributions and standard errors of the wildtype and three mutants, during the final 1 ns of the simulations, are provided in Table I. The energies associated with the solvent accessibility surface area of the catalytic cleft are also provided in kcal/mol.

DISCUSSION

We present the first detailed mechanistic hypotheses at the atomic level that suggest possibilities of how three cancer-related kinase and helical domain mutations seen in human breast and other cancers may hyperactivate the PI3K pathway. Using homology modeling and LD simulations, we find evidence that the H1047R/L mutants and P539R mutants could induce hyperactivation through two different molecular mechanisms, as indicated by differences in solvent accessible surface area of the catalytic cleft, activation loop mobility, and thermostability (Table II). Understanding the potential biochemical and medical utility of homology models is particularly relevant in the light of funding agencies' assessment of structural genomics initiatives.[50] Our study suggests that by combining LD, homology models, and ligand docking, it is possible to develop medically relevant hypotheses about protein function and potential inhibitors, when experimentally determined structures are not available. Importantly, these hypotheses need to be validated or discredited by further experimental studies. However, a "two mechanism" hypothesis consistent with our results was recently proposed and supported by biochemical studies in chicken embryo fibroblasts. PIK3CA hotspot double mutants in the helical domain (E542K, E545K) had additive effects on oncogenic transformation, whereas those with mutations in both helical and kinase domains (E542K, H1047R), (E545K, H1047R) had multiplicative effects.[51]

The existence of two or more molecular mechanisms for PIK3CA hyperactivation of the PI3K pathway suggests the possibility that inhibitors could be designed to target specific mutations.[51] The past 5 years have seen great progress in pharmaceutical efforts to develop PI3K inhibitors, and several hundred candidate small molecules have been patented. Many are isoform-specific and thus have the potential to minimize side effects and toxicity

produced by pan-PI3K inhibitors[52] such as Wortmannin[53] and LY294002.[54] These drugs were unable to enter clinical trials due to issues with liver toxicity and dermal toxicity.[54,55] Developing PIK3CA mutation-specific inhibitors could further minimize side effects by taking advantage of conformational differences among particular mutants and wildtype.[51]

Kinase domain mutants H1047R/L

The larger solvent accessible surface area of the catalytic cleft observed only in H1047R and H1047L has the potential to facilitate the entrance of substrates (ATP and PIP_2) when compared with wildtype. This event could cause PIK3CA mutants with the capability for faster substrate-to-product (PIP_3) turnover. However, this possible correlation needs to be tested experimentally. Importantly, the relationship between kinase catalytic subunit dynamics and catalysis, in general, is an open and active area of research.[56] Many PI3K inhibitors have been developed on the model of protein kinase inhibitors, which generally compete with ATP for the ATP-binding pocket.[52] If our hypothesis about increased accessibility to this pocket in H1047R/L mutants is experimentally validated, these mutant PIK3CAs may have increased sensitivity to ATP-competitive inhibitors. In our simulations, the H1047R mutant also exhibits a flip of the phenylalanine (F934) and aspartic acid (D933) residues in the conserved DFG motif, with respect to its preferred orientation in the wildtype (see Fig. 5). In the flipped position, F934 becomes more exposed to substrates entering the catalytic cleft. This altered conformation (if validated) could possibly be exploited. A competitive ATP binding inhibitor capable of stronger interactions with H1047R's more exposed hydrophobic F934 residue might have lower IC_{50} values for inhibition of the H1047R mutant than wildtype. Because the D933 residue, in the absence of ATP, is accessible to solvent, it is possible that it may also be involved in hydrogen bonding with a water molecule. We plan to explore this possibility in our future work with the X-ray crystal structure.

Activation loop mobility

The activation loop acts like a string connecting a hinge region close to position 1047 to the DFG motif near the catalytic loop. Our simulations show that perturbations in the activation loop by arginine and leucine substitutions propagate across activation and catalytic loops to the catalytic cleft. One possibility is that this propagation could be constrained by an inhibitor that is a strong electrophile and would directly attack the lysine-rich nucleophilic region of the activation loop.

Helical domain mutant P539R

In our simulations, the P539R mutant (and to a lesser extent, the H1047R/L mutants) exhibit an increase in the number of hydrogen bonds and salt-bridge interactions, compared with the wildtype. These quantities are associated with increased protein thermostability.[57,58] Previous studies have pointed to the possibility of a protein-dependent correlation between metabolic stability and thermostability.[59,60] If such a correlation exists for PIK3CA, mutants that increase thermostability would also have a longer half-life in the cell, yielding a higher concentration of PIK3CAs. In this scenario, gain-of-function would no longer be primarily at the level of an individual PIK3CA molecule, but would be a result of having a larger number of active, PIP_3-producing PIK3CA molecules. We speculate that the F934 targeted inhibitor designed for H1047R mutants might not be the best choice for patients with a P539R mutation.

Our simulations have suggested ideas about how mutation-specific changes in conformation could be exploited for drug development, but we emphasize that the work in this study is preliminary. To adequately gather information about all the correlated motions among residues in a large protein like PIK3CA (1000+ amino acid residues) requires more

extensive simulations. Now that an X-ray crystal structure of PIK3CA, in complex with the niSH2 domain (residues 322–600) of p85α has been published, we are using it as the starting conformation for subsequent work.

Experimental validation

We have presented several hypotheses concerning conformational changes that distinguish among wildtype PIK3CA and three hot-spot mutants commonly seen in human tumors. To validate or discredit these hypotheses will require further biophysical studies.

Kinase lobe separations—The increased solvent accessible surface area of the catalytic cleft in the H1047R/L mutants, compared with wildtype and P539R, could be checked using iodide quenching of fluorescence or single molecule Forster resonance energy transfer (FRET).[61,62] For example, using FRET, the N- and C-lobes of each species could be labeled with selectively attached fluorophores, and intensities and interlobe distances could be measured with the Förster theory of FRET.[63]

Increased thermostability—The increased thermostability of P539R and H1047R/L mutants with respect to wildtype could be tested using either differential scanning calorimetry or chemical denaturation experiments. Differential scanning calorimetry evaluates the unfolding enthalpies and associated heat capacity changes accompanying thermal denaturation.[64] The measured melting temperatures allow the comparison of thermostability of one structure versus another.

P539R and helical-C2 domain interactions—The relationship of increased electrostatic attraction between helical and C2 domains (E453 and R539) (see Fig. 4) and oncogenicity can be tested with double-mutation studies. If replacing E453 with a basic or bulky non-polar residue decreases phosphorylation levels of AKT and S6K and cell transformation (focus formation),[51] then the P539R mutation is likely involved in modifying interdomain associations.

Phenylalanine flip—The structural flexibility of the phenylalanine residue in the DFG motif can be investigated through fluorescence decay measurements using a 265 nm AlGaN light-emitting diode.[65]

CONCLUSIONS

Little is known about why and how PIK3CA somatic mutations found in breast and other solid tumors contribute to inducing gain of function in PI3K-related molecular pathways. We have presented some possible gain-of-function mechanisms that might result from three mutations found in the helical and kinase domains of PIK3CA. The validity of our hypotheses awaits the results of further experimental studies.

Acknowledgments

Grant sponsor: Susan G. Komen Foundation award; Grant number: KG080137; Grant sponsor: Department of Defense; Grant number: COE W81XWH-04-1-0595; Grant sponsor: SPORE; Grant number: P50CA88843.

We thank Dr. Tom Keyes and Boston University Supercomputing staff for allowing us access to the BU supercomputing facilities and Dr. Lewyn Li for valuable discussions.

References

1. Karakas B, Bachman KE, Park BH. Mutation of the PIK3CA oncogene in human cancers. Br J Cancer. 2006; 94:455–459. [PubMed: 16449998]

2. Bachman KE, Argani P, Samuels Y, Silliman N, Ptak J, Szabo S, Konishi H, Karakas B, Blair BG, Lin C, Peters BA, Velculescu VE, Park BH. The PIK3CA gene is mutated with high frequency in human breast cancers. Cancer Biol Ther. 2004; 3:772–775. [PubMed: 15254419]

3. Liang X, Lau QC, Salto-Tellez M, Putti TC, Loh M, Sukumar S. Mutational hotspot in exon 20 of PIK3CA in breast cancer among Singapore Chinese. Cancer Biol Ther. 2006; 5:544–548. [PubMed: 16582596]

4. Bader AG, Kang S, Vogt PK. Cancer-specific mutations in PIK3CA are oncogenic in vivo. Proc Natl Acad Sci USA. 2006; 103:1475–1479. [PubMed: 16432179]

5. Zhao JJ, Liu Z, Wang L, Shin E, Loda MF, Roberts TM. The oncogenic properties of mutant p110alpha and p110beta phosphatidylinositol 3-kinases in human mammary epithelial cells. Proc Natl Acad Sci USA. 2005; 102:18443–18448. [PubMed: 16339315]

6. Isakoff SJ, Engelman JA, Irie HY, Luo J, Brachmann SM, Pearline RV, Cantley LC, Brugge JS. Breast cancer-associated PIK3CA mutations are oncogenic in mammary epithelial cells. Cancer Res. 2005; 65:10992–11000. [PubMed: 16322248]

7. Engelman JA, Luo J, Cantley LC. The evolution of phosphatidylinositol 3-kinases as regulators of growth and metabolism. Nat Rev Genet. 2006; 7:606–619. [PubMed: 16847462]

8. Wymann MP, Pirola L. Structure and function of phosphoinositide 3-kinases. Biochim Biophys Acta. 1998; 1436:127–150. [PubMed: 9838078]

9. Walker EH, Perisic O, Ried C, Stephens L, Williams RL. Structural insights into phosphoinositide 3-kinase catalysis and signalling. Nature. 1999; 402:313–320. [PubMed: 10580505]

10. Forbes S, Clements J, Dawson E, Bamford S, Webb T, Dogan A, Flanagan A, Teague J, Wooster R, Futreal PA, Stratton MR. Cosmic 2005. Br J Cancer. 2006; 94:318–322. [PubMed: 16421597]

11. Gymnopoulos M, Elsliger MA, Vogt PK. Rare cancer-specific mutations in PIK3CA show gain of function. Proc Natl Acad Sci USA. 2007; 104:5569–5574. [PubMed: 17376864]

12. Saal LH, Holm K, Maurer M, Memeo L, Su T, Wang X, Yu JS, Malmstrom PO, Mansukhani M, Enoksson J, Hibshoosh H, Borg A, Parsons R. PIK3CA mutations correlate with hormone receptors, node metastasis, and ERBB2, and are mutually exclusive with PTEN loss in human breast carcinoma. Cancer Res. 2005; 65:2554–2559. [PubMed: 15805248]

13. Kang S, Bader AG, Vogt PK. Phosphatidylinositol 3-kinase mutations identified in human cancer are oncogenic. Proc Natl Acad Sci USA. 2005; 102:802–807. [PubMed: 15647370]

14. Samuels Y, Diaz LA Jr, Schmidt-Kittler O, Cummins JM, Delong L, Cheong I, Rago C, Huso DL, Lengauer C, Kinzler KW, Vogelstein B, Velculescu VE. Mutant PIK3CA promotes cell growth and invasion of human cancer cells. Cancer Cell. 2005; 7:561–573. [PubMed: 15950905]

15. Wu G, Xing M, Mambo E, Huang X, Liu J, Guo Z, Chatterjee A, Goldenberg D, Gollin SM, Sukumar S, Trink B, Sidransky D. Somatic mutation and gain of copy number of PIK3CA in human breast cancer. Breast Cancer Res. 2005; 7:R609–R616. [PubMed: 16168105]

16. Huse M, Kuriyan J. The conformational plasticity of protein kinases. Cell. 2002; 109:275–282. [PubMed: 12015977]

17. Pirola L, Zvelebil MJ, Bulgarelli-Leva G, van Obberghen E, Waterfield MD, Wymann MP. Activation loop sequences confer substrate specificity to phosphoinositide 3-kinase alpha (PI3Kalpha). Functions of lipid kinase-deficient PI3Kalpha in signaling. J Biol Chem. 2001; 276:21544–21554. [PubMed: 11278889]

18. Cheng Y, Zhang Y, McCammon JA. How does activation loop phosphorylation modulate catalytic activity in the cAMP-dependent protein kinase: a theoretical study. Protein Sci. 2006; 15:672–683. [PubMed: 16522793]

19. Liu Y, Belkina NV, Graham C, Shaw S. Independence of protein kinase C-delta activity from activation loop phosphorylation: structural basis and altered functions in cells. J Biol Chem. 2006; 281:12102–12111. [PubMed: 16505477]

20. Liu Y, Purvis J, Shih A, Weinstein J, Agrawal N, Radhakrishnan R. A multiscale computational approach to dissect early events in the erb family receptor mediated activation, differential signaling, and relevance to oncogenic transformations. Ann Biomed Eng. 2007; 35:1012–1025. [PubMed: 17273938]

21. Ikenoue T, Kanai F, Hikiba Y, Obata T, Tanaka Y, Imamura J, Ohta M, Jazag A, Guleng B, Tateishi K, Asaoka Y, Matsumura M, Kawabe T, Omata M. Functional analysis of PIK3CA gene mutations in human colorectal cancer. Cancer Res. 2005; 65:4562–4567. [PubMed: 15930273]
22. Wallner B, Elofsson A. All are not equal: a benchmark of different homology modeling programs. Protein Sci. 2005; 14:1315–1327. [PubMed: 15840834]
23. Wallner B, Elofsson A. Identification of correct regions in protein models using structural, alignment, and consensus information. Protein Sci. 2006; 15:900–913. [PubMed: 16522791]
24. Capener CE, Shrivastava IH, Ranatunga KM, Forrest LR, Smith GR, Sansom MS. Homology modeling and molecular dynamics simulation studies of an inward rectifier potassium channel. Biophys J. 2000; 78:2929–2942. [PubMed: 10827973]
25. Sansom MS, Shrivastava IH, Bright JN, Tate J, Capener CE, Biggin PC. Potassium channels: structures, models, simulations. Biochim Biophys Acta. 2002; 1565:294–307. [PubMed: 12409202]
26. Szklarz GD, Paulsen MD. Molecular modeling of cytochrome P450 1A1: enzyme-substrate interactions and substrate binding affinities. J Biomol Struct Dyn. 2002; 20:155–162. [PubMed: 12354067]
27. Arora K, Brooks CL III. Large-scale allosteric conformational transitions of adenylate kinase appear to involve a population-shift mechanism. Proc Natl Acad Sci USA. 2007; 104:18496–18501. [PubMed: 18000050]
28. Gohlke H, Kiel C, Case DA. Insights into protein-protein binding by binding free energy calculation and free energy decomposition for the Ras-Raf and Ras-RalGDS complexes. J Mol Biol. 2003; 330:891–913. [PubMed: 12850155]
29. Zhou R, Friesner RA, Ghosh A, Rizzo RC, Jorgensen WL. New linear interaction method for binding affinity calculations using a continuum solvent model. J Phys Chem B. 2001; 105:10388–10397.
30. Sali A, Blundell TL. Comparative protein modelling by satisfaction of spatial restraints. J Mol Biol. 1993; 234:779–815. [PubMed: 8254673]
31. Sanchez R, Sali A. Large-scale protein structure modeling of the *Saccharomyces cerevisiae* genome. Proc Natl Acad Sci USA. 1998; 95:13597–13602. [PubMed: 9811845]
32. Eswar N, John B, Mirkovic N, Fiser A, Ilyin VA, Pieper U, Stuart AC, Marti-Renom MA, Madhusudhan MS, Yerkovich B, Sali A. Tools for comparative protein structure modeling and analysis. Nucleic Acids Res. 2003; 31:3375–3380. [PubMed: 12824331]
33. Clamp M, Cuff J, Searle SM, Barton GJ. The Jalview Java alignment editor. Bioinformatics (Oxford England). 2004; 20:426–427.
34. Fiser A, Do RK, Sali A. Modeling of loops in protein structures. Protein Sci. 2000; 9:1753–1773. [PubMed: 11045621]
35. Shen MY, Sali A. Statistical potential for assessment and prediction of protein structures. Protein Sci. 2006; 15:2507–2524. [PubMed: 17075131]
36. Melo F, Devos D, Depiereux E, Feytmans E. ANOLEA: a www server to assess protein structures. Proc Int Conf Intell Syst Mol Biol. 1997; 5:187–190. [PubMed: 9322034]
37. Sippl MJ. Recognition of errors in three-dimensional structures of proteins. Proteins. 1993; 17:355–362. [PubMed: 8108378]
38. MacKerell AD, Bashford D, Bellott M, Dunbrack JR, Evanseck J, Field MJ, Fischer S, Gao J, Guo H, Ha S, Joseph D, Kuchnir L, Kuczera AK, Lau FTK, Mattos C, Michnick S, Ngo T, Nguyen DT, Prodhom B, Reiher IWE, Roux B, Schlenkrich M, Smith JC, Stote R, Straub J, Watanabe M, Wiorkiewicz-Kuczera J, Yin D, Karplus M. All-atom empirical potential for molecular modeling and dynamics studies of proteins. J Phys Chem B. 1998; 102:3586–3616.
39. Lee MS, Feig M, Salsbury FR Jr, Brooks CL III. New analytic approximation to the standard molecular volume definition and its application to generalized Born calculations. J Comput Chem. 2003; 24:1348–1356. [PubMed: 12827676]
40. Dominy BN, Brooks CL. Identifying native-like protein structures using physics-based potentials. J Comput Chem. 2002; 23:147–160. [PubMed: 11913380]
41. Feig M. Kinetics from implicit solvent simulations of biomolecules as a function of viscosity. J Chem Theory Comput. 2007; 3:1734–1748.

42. Feig M, Chocholousova J, Tanizaki S. Extending the horizon: towards the efficient modeling of large biomolecular complexes in atomic detail. Theor Chem Acc. 2006; 116:194–205.
43. Feig M, Brooks CL. Recent advances in the development and application of implicit solvent models in biomolecule simulations. Curr Opin Struct Biol. 2004; 14:217–224. [PubMed: 15093837]
44. Ryckaert JP, Ciccotti G, Berendsen HJC. Numerical integration of the Cartesian equations of motion of a system with constraints: molecular dynamics of n-alkanes. J Comput Phys. 1977; 23:327–341.
45. Brooks BR, Bruccoleri RE, Olafson BD, States DJ, Swaminathan S, Karplus M. CHARMM: a program for macromolecular energy, minimization and dynamics calculations. J Comput Chem. 1983; 4:187–217.
46. Huang CH, Mandelker D, Schmidt-Kittler O, Samuels Y, Velculescu VE, Kinzler KW, Vogelstein B, Gabelli SB, Amzel LM. The structure of a human p110alpha/p85alpha complex elucidates the effects of oncogenic PI3Kalpha mutations. Science. 2007; 318:1744–1748. [PubMed: 18079394]
47. Davis AM, Teague SJ, Kleywegt GJ. Application and limitations of X-ray crystallographic data in structure-based ligand and drug design. Angew Chem Int Ed. 2003; 42:2718–2736.
48. Foster FM, Traer CJ, Abraham SM, Fry MJ. The phosphoinositide (PI) 3-kinase family. J Cell Sci. 2003; 116(Pt 15):3037–3040. [PubMed: 12829733]
49. Knight ZA, Gonzalez B, Feldman ME, Zunder ER, Goldenberg DD, Williams O, Loewith R, Stokoe D, Balla A, Toth B, Balla T, Weiss WA, Williams RL, Shokat KM. A pharmacological map of the PI3-K family defines a role for p110alpha in insulin signaling. Cell. 2006; 125:733–747. [PubMed: 16647110]
50. Service RF. Structural biology. Protein structure initiative: phase 3 or phase out. Science. 2008; 319:1610–1613. [PubMed: 18356501]
51. Zhao L, Vogt PK. Helical domain and kinase domain mutations in p110alpha of phosphatidylinositol 3-kinase induce gain of function by different mechanisms. Proc Natl Acad Sci USA. 2008; 105:2652–2657. [PubMed: 18268322]
52. Marone R, Cmiljanovic V, Giese B, Wymann MP. Targeting phosphoinositide 3-kinase: moving towards therapy. Biochim Biophys Acta. 2008; 1784:159–185. [PubMed: 17997386]
53. Okada T, Sakuma L, Fukui Y, Hazeki O, Ui M. Blockage of chemotactic peptide-induced stimulation of neutrophils by wortmannin as a result of selective inhibition of phosphatidylinositol 3-kinase. J Biol Chem. 1994; 269:3563–3567. [PubMed: 8106399]
54. Vlahos CJ, Matter WF, Hui KY, Brown RF. A specific inhibitor of phosphatidylinositol 3-kinase, 2-(4-morpholinyl)-8-phenyl-4H-1-benzopyran-4-one (LY294002). J Biol Chem. 1994; 269:5241–5248. [PubMed: 8106507]
55. Ihle NT, Williams R, Chow S, Chew W, Berggren MI, Paine-Murrieta G, Minion DJ, Halter RJ, Wipf P, Abraham R, Kirkpatrick L, Powis G. Molecular pharmacology and antitumor activity of PX-866, a novel inhibitor of phosphoinositide-3-kinase signaling. Mol Cancer Ther. 2004; 3:763–772. [PubMed: 15252137]
56. Johnson DA, Akamine P, Radzio-Andzelm E, Madhusudan M, Taylor SS. Dynamics of cAMP-dependent protein kinase. Chem Rev. 2001; 101:2243–2270. [PubMed: 11749372]
57. Vogt G, Woell S, Argos P. Protein thermal stability, hydrogen bonds, and ion pairs. J Mol Biol. 1997; 269:631–643. [PubMed: 9217266]
58. Vogt G, Argos P. Protein thermal stability: hydrogen bonds or internal packing? Fold Des. 1997; 2:S40–S46. [PubMed: 9269567]
59. Inoue I, Rechsteiner M. On the relationship between the metabolic and thermodynamic stabilities of T4 lysozymes. Measurements in eukaryotic cells. J Biol Chem. 1994; 269:29247–29251. [PubMed: 7961893]
60. Almog O, Gallagher DT, Ladner JE, Strausberg S, Alexander P, Bryan P, Gilliland GL. Structural basis of thermostability. Analysis of stabilizing mutations in subtilisin BPN′. J Biol Chem. 2002; 277:27553–27558. [PubMed: 12011071]
61. Ha T, Enderle T, Ogletree DF, Chemla DS, Selvin PR, Weiss S. Probing the interaction between two single molecules: fluorescence resonance energy transfer between a single donor and a single acceptor. Proc Natl Acad Sci USA. 1996; 93:6264–6268. [PubMed: 8692803]

62. Ablooglu AJ, Frankel M, Rusinova E, Ross JB, Kohanski RA. Multiple activation loop conformations and their regulatory properties in the insulin receptor's kinase domain. J Biol Chem. 2001; 276:46933–46940. [PubMed: 11598120]

63. Forster T. Zwischenmolekulare Energiewanderung und Fluoreszenz. Ann Phys. 1948; 2:55–70.

64. Dean, JA. The analytical chemistry handbook. New York: McGraw Hill; 1995. p. 5

65. McGuiness DC, Macmillan AM, Sagoo K, McLoskey D, Birch DJS. Excitation of fluorescence decay using a 265 nm pulsed light-emitting diode: evidence for aqueous phenylalanine rotamers. Appl Phys Lett. 2006; 89:3.

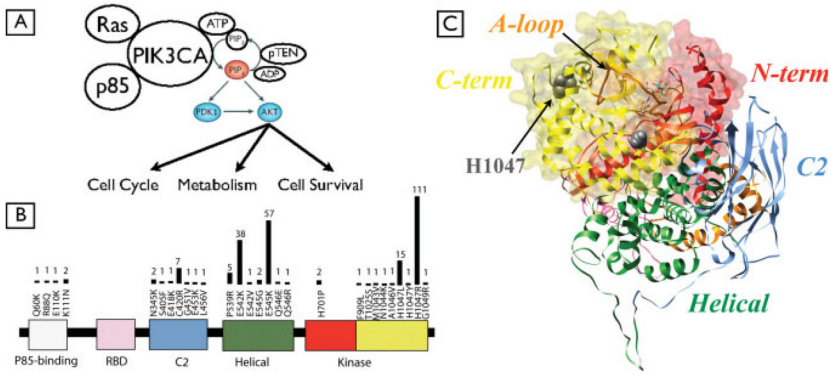

Figure 1.

PI3K signaling pathway, PIK3CA breast cancer-derived somatic mutations and homology model: (**A**) PIK3CA converts PIP_2 to PIP_3, whereas the phosphatase PTEN converts PIP_3 back to PIP_2. PIP_3 acts as a second messenger, binding to the tyrosine kinase AKT, and activating many downstream pathways[7]; (**B**) Schematic diagram of PIK3CA protein illustrating functional domains and some somatic mutations found in breast cancer (frequencies from COSMIC database[10]). The three hotspot mutations are E542K, E545K, and H1047R. RBD refers to Ras-binding domain; (**C**) The kinase domain N- and C-lobes are shown with transparent surfaces. Here, we show the ATP as it is positioned in PIK3CG, in the cleft between kinase N- and C-lobes. The activation loop, which is partially disordered in the PIK3CG crystal structures, is shown before minimization and equilibration in CHARMM. The long loops are linkers between C2-RBD and C2-helical domains that are disordered in the crystal structures. These linkers are distal from the catalytic domain and do not seem to impact the activation loop and kinase lobe motions studied here.

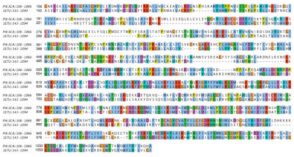

Figure 2.
Alignment used to build the homology model of PIK3CA. Target-template alignment of human PIK3CA and porcine PIK3CG built by ModPipe2.[32] Alignment rendered in Jalview 2.3.[33] [Color figure can be viewed in the online issue, which is available at www.interscience.wiley.com.]

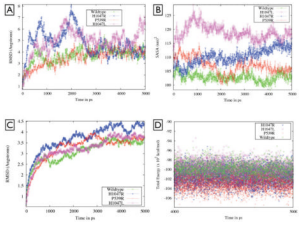

Figure 3.

Local structural variations of activation loop, catalytic domain and PIK3CA global structural variation: (**A**) The root-mean-squared deviation (RMSD) of the activation loop for wildtype PIK3CA and H1047R/L and P539R mutants shows the higher loop mobility for H1047R/L; (**B**) The solvent accessible surface area (SASA) of the catalytic cleft of PIK3CA. The H1047R and H1047L mutants show much higher solvent accessible surface area, compared with the wildtype and the P539R mutant; (**C**) RMSD of the main chain backbone atoms relative to the corresponding structure at 0 ns for the wildtype and mutants as a function of the simulation time. The RMSD reaches a stable average after 3.25 ns; (**D**) The total converged energies of wildtype and the three mutants over the last 1 ns of the time trajectories are shown.

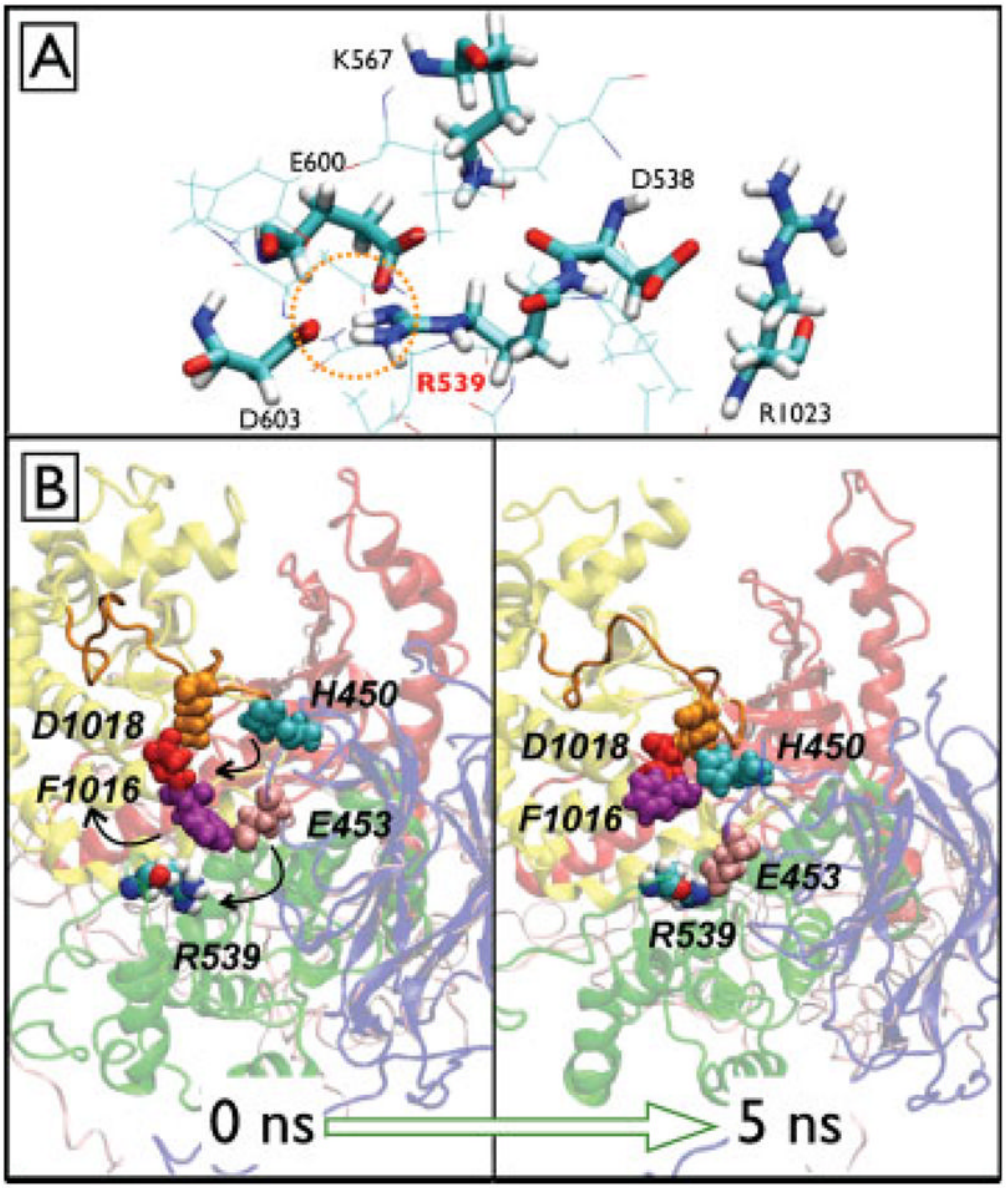

Figure 4.

Electrostatic impact of P539R mutation includes formation of a salt-bridge triad and altered interdomain packing: (**A**) R539 forms salt-bridging interactions with D603 and E600. These interactions do not occur in the wildtype; (**B**) Over the time course of this simulation, E453 (C2 domain) develops an electrostatic interaction with R539. Consequently, F1016 (kinase domain) moves away from the tri-domain (C2, helical and kinase) interface, whereas H450 (C2 domain) moves towards D1018 (kinase domain). The overall effect of these conformational changes pulls the C2 domain closer to the helical domain. [Color figure can be viewed in the online issue, which is available at www.interscience.wiley.com.]

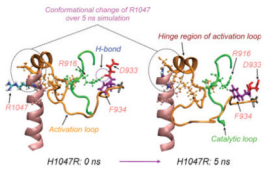

Figure 5.

Hypothetical mechanism of F934 “flip” conformation in H1047R mutant: the conformational change in R1047 perturbs the hinge region of the activation loop (orange) and subsequently reorganizes the network of interactions between activation loop and catalytic loop (green). At 0 ns, R916 in the catalytic loop forms a hydrogen bond with D933 of the DFG motif. At 5 ns, this bond is broken, resulting in a ~90° rotation of D933. As a result, F934 which originally pointed towards the interior of the protein, flips and becomes more exposed.

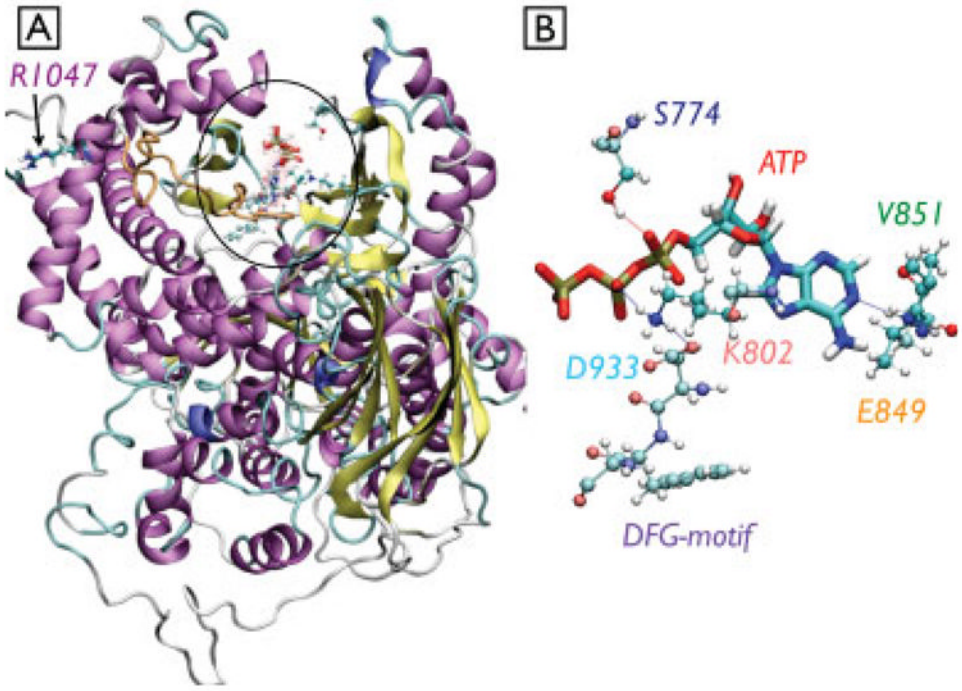

Figure 6.

Model of PIK3CA H1047R mutant with bound ATP: (**A**) Circle denotes binding site of ATP in the catalytic cleft. Activation loop shown in orange; (**B**) Details of ATP binding in the model. The ATP forms hydrogen bonds with V851, S774, E849, and K802. The D933 of the DFG motif forms a salt bridge with K802. [Color figure can be viewed in the online issue, which is available at www.interscience.wiley.com.]

Table I

Energy Contributions in PIK3CA Simulations

Energy contributions	Wildtype	P539R	H1047L	H1047R
MM energy	−8597.8 ± 2.6	−9941.3 ± 2.1	−7655.0 ± 4.8	−9169.2 ± 2.6
GBMV	−13148.1 ± 1.8	−12081.7 ± 1.8	−14093.3 ± 9.2	−12706.9 ± 2.4
SASA	430.28 ± 1.4	444.19 ± 0.9	518.12 ± 1.8	481.6 ± 1.0

Average energies and standard errors for wildtype and the three mutants are reported in units of kcal/mol.

MM, molecular mechanics ($E_{MM} = E_{bond} + E_{bend} + E_{Urey\text{-}Bradley} + E_{dihedral} + E_{Improper} + E_{vdW} + E_{elec}$); GBMV, generalized born molecular volume; SASA, solvent accessible surface area.

Table II

Differences in Structural Properties of PIK3CA H1047R, H1047L, and P539R Mutants Compared with Wildtype Control

	Wildtype	H1047R/L	P539R
Catalytic cleft SASA	No	Yes	No
Activation loop mobility	No	Yes	No
Thermostability	No	Yes	Yes

SASA, solvent accessible surface area.